

# UVM ScholarWorks

## Polarization and Pulsars

Item Type	undergrad_thesis;article;undergraduate thesis
Authors	Brinkman, Casey Lynn
Download date	2026-05-13 09:45:51
Link to Item	<a href="https://hdl.handle.net/20.500.14849/513">https://hdl.handle.net/20.500.14849/513</a>

# Polarization and Pulsars: Traditional Vector Models and the Mode Switching Phenomena

Casey Lynn Brinkman

Spring 2017

## **Abstract**

The phenomenon of profile mode switching in pulsars, where the stable average pulse profile changes to another stable state on the timescale of a pulsar's period, is not well understood. Through my research, I sought to understand how pulsars undergo profile mode switching by an analysis of the polarization across different profile modes of PSR B0329+54. A hypothesized change in rotation vector model parameters between the modes would indicate changes in coherent emission process, a possible source of mode switching. We reject this hypothesis, and instead support a model of pair production in the surface plasma that would cause a change in the available electrons and therefore pulsar intensity. I couple this with the timing solutions for twelve Arecibo pulsars, and a polarization analysis of each in order to construct a comprehensive look at different aspects of pulsar polarimetry.

# 1 Introduction

## 1.1 About Pulsars

A star spends its lifetime fusing hydrogen into heavier elements—balancing energy output precariously with the force of gravity—until the fuel to sustain a star runs out. When a star dies several different fates await, depending on the mass of the star: stars between 0-1.4 times the mass of the sun turn into a white dwarf star, yet stars much more than three times the mass of the sun will become black holes. In between these two fates lies the realm of neutron stars: the material of the star has collapsed so drastically under its own gravity that the electrons and protons have been pressed into neutrons, finding stability with neutron degenerate gas pressure (Lorimer & Kramer (2004)).

Neutron stars rotate rapidly—anywhere from 10 seconds per period all the way down to millisecond periods—and have magnetic fields over a billion times stronger than that of the sun. A potential gap forms at the magnetic poles, which sparks the production of relativistic  $\gamma$  particles. These particles further radiate as they move through the magnetic field, pair producing electrons and positrons, which are in turn radiating to produce more photons, which produce more electrons and positrons. This cycle is called an electron cascade process. As these electrons move along the curved magnetic field, they produce curvature radiation which results in a beam of light radiating from the star's magnetic poles. The emission we see from pulsars is coherent, which means that we assume no phase difference between the individual

electrons that compose the charge, and the overall charge  $Q \approx N^2e$  where  $N$  is the number of electrons (Mitra et al. (2015)). As these stars rotate through our line of sight, we see this as a bright pulse of emission, just as we see the bright pulses of light from a rotating lighthouse.

These Pulsing Radio Sources, or more succinctly “Pulsars,” were first discovered by Jocelyn Bell in 1967 and later became identified as these rapidly rotating neutron stars. Pulsar names are denoted by either a B or J, to indicate which catalogue they belong to, and their coordinates (Right Ascension + Declination) (Lorimer & Kramer (2004)). The regularity of a star’s pulses can be used to keep time so meticulously it rivals the precision of atomic clocks, and the extreme densities and magnetic field strengths make pulsars some of the most extreme physics laboratories to exist; and yet, most phenomena on pulsars remains shrouded in mystery. All of these make pulsar research an important and curiosity-fulfilling pursuit, and my thesis will touch on all three of these aspects in order to give a comprehensive interpretation of pulsars—primarily through the lens of polarization.

## **1.2 My Project**

### **1.2.1 Timing**

Since the discovery of the first radio pulsar in 1967, more than 2500 pulsars have been discovered. Of these, more than 400 do not have published phase-coherent timing solutions: a set of parameters such as period of rotation that can be determined for

a pulsar, and then applied across gaps in observation. Similarly, many newly discovered pulsars lack average polarimetry and fluctuation-spectral analysis. I looked at a group of twelve previously discovered pulsars in order to calculate their timing parameters, estimate the geometry of the emission, and analyze the polarization characteristics of each. These pulsars are relatively bright, and for that reason were used as test pulsars during the very early demonstration stages of the Arecibo 327-MHz drift scan survey, but they have never had formal analyses published. This work will allow us to gain a more comprehensive understanding of pulsars in general, and will help us distinguish the unusual ways in which pulsars sometimes behave.

The twelve pulsars I used for timing and polarimetry were all discovered with the 430-MHz line feed of the Arecibo 305-m radio telescope in Puerto Rico. Most were discovered in drift-scan surveys: two, J0943+22 and J1246+22, were reported by Thorsett et al in 1993, while three others (J0435+27, J0927+23, J0947+27) were discovered in the completion of that survey by Ray et al. in 1996. Five further pulsars (J0517+22, J0627+07, J1404+12, J1935+12 and J1938+22) were first discovered by Chandler in 2003, but again no timing solutions were presented for them. Two other pulsars (J1756+18 and J2050+13) were discovered in the Arecibo 430-MHz intermediate latitude survey by Navarro et al in 2003, but without timing solutions. Finally, in Ray et al in 1996, an additional pulsar candidate (J2052+17) was listed, but the authors were unable to confirm it because of the start of the Arecibo upgrade. In 2004 October, Paulo Freire confirmed the existence of this pulsar with the 327 MHz Gregorian receiver of the 305-m Arecibo radio telescope and the Wideband Arecibo Pulsar Processors (hereafter WAPPs).

The UVM astrophysics department does not focus on pulsar timing, so I conducted this work with Paulo Freire at the Max Planck Institute fur Radioastronomie in Bonn, Germany. We present phase-coherent timing solutions for these pulsars, including precise measurements of their position, period, rate of spin down, dispersion measure, age, magnetic field, and distance from Earth. Pulsar timing work is most famous for its role in the search for gravitational waves; however, precise timing parameters are also used in determining the emission geometry and polarization model parameters.

### 1.2.2 Polarimetry

One of the most important tools we can use to unlock the physics of pulsars is polarization. The amount of linear and circular polarization, as well as the angles at which they arrive, can tell us information about the magnetic fields where the emission has been generated. Through the study of the Vela pulsar, Radhakrishnan and Cooke (1969) showed how the linear polarization position angle usually rotates across the center of the pulse in an “S” shape, establishing a rotating vector model (or RVM) to which many pulsars adhere. The traverse of the polarization angle in the RVM arises from the varying projected magnetic field direction within an overall dipole configuration. The position angle  $\chi$  as a function of pulse longitude  $\phi$  can be expressed as:

$$\chi = \tan^{-1} \frac{\sin(\alpha)\sin(\phi)}{\sin(\alpha+\beta)\cos(\alpha) - \sin(\alpha)\cos(\alpha+\beta)\cos(\phi)}$$

A survey of these pulsars shows the similarities in the properties and behavior of most pulsars; however, it also highlights a number of strange phenomena, such as interpulses, drifting subpulses, and pulse nulling (a full description of these phenomena will be presented in the analysis section). Much of pulsar research focuses on creating the rules which most pulsars follow, but the rule breaking pulsars are often the most interesting to try and understand. One of the most curious rule-breaking phenomena is known as profile mode switching, and in order to investigate this further we turn our attention to a very unique pulsar: B0329+54.

### **1.2.3 B0329+54**

The emission we receive from pulsars normally follows a pulse profile: while individual pulses may look radically different, the average of any section of pulses will look the same. However, not every pulsar follows a single profile and will spend varying amounts of time switching between two or more different profiles. The phenomenon of profile mode switching was first observed in PSR B1237+25 by Backer in 1970, which was subsequently followed by the discovery of mode switching in PSR B0329+54 by Lyne in 1971. I drew inspiration from a paper by Bartel et al from 1982 investigating B0329+54 and comparing the two modes in terms of time spent in each mode, the ratios of intensity between the two modes, and much more. They discuss various proposed methods of mode switching, and lean toward a model proposed by Ruderman and Sutherland in 1975, which holds quantum changes in the neutron plasma responsible.

The reason for mode switching, however, has remained mysterious. There are ways to eliminate certain models and give support to others, which is what we seek to do through a geometric and polarimetric analysis. Differences in the emission height or polarization position angle traverse in the central component between modes would tell us that some aspect of the emission mechanism is responsible for the differences in profile shape between modes. However, if we find no difference in the solution to the rotation vector model, it tells us that the phenomena is most likely a result of pair production changes in the neutron plasma in the sparking regions.

Professors Dipanjan Mitra, Joanna Rankin, and Yashwant Gupta of the National Centre for Radio Astrophysics in Pune, India published Absolute broad-band polarization behavior of PSR B0329+54: a glimpse of the core emission process in 2007, in which they studied the radio wave polarization from this pulsar as a function of intensity and frequency to investigate an unusual arc in the polarization position angle called the “kink”. The core emission has unique intensity dependence: low-intensity pulses follow the typical rotation vector model for circular polarization, while the circular polarization rotates at a steeper angle for higher intensity pulses.

Because this pulsar has such unusual and distinct core polarization behavior, it provides a very transparent way to compare the core emission between the modes: my project looks at the abnormal mode of this pulsar to see if the same arc in circular polarization is present in the core component of the emission as there is in the normal mode. Then, I will look at the differences between total linear and circular polarization between the modes as well as the height of emission in order to identify all possible similarities and differences.

## 2 Methodology

### 2.1 Timing

For Pulsar timing we used data collected remotely from Arecibo. I used a program called TEMPO (created by members of the NANOGrav organization) and ran it for each of the files in order to produce the frequency and frequency derivatives for each pulsar. From there, I used the frequency to calculate dispersion measure, age, magnetic field, energy loss rate, and distance from Earth using formulas found in Lorimer.

TEMPO gives rotation frequency, its derivative, dispersion measure (or an estimation of how dispersed the pulse has become while traveling through the interstellar medium) and the coordinates in right ascension and declination. Using these values I calculated the following parameters.

The galactic coordinates  $b$  and  $l$  as:

$$\begin{aligned}\cos(b) \cos(l - 33^\circ) &= \cos(\delta) \cos(\alpha - 282.25^\circ) \\ \cos(b) \sin(l - 33^\circ) &= \sin(\delta) \sin(62.6^\circ) + \cos(\delta) \sin(\alpha - 282.25^\circ) \cos(62.6^\circ)\end{aligned}$$

In order to calculate the rest of the parameters, I needed to transform rotation and its derivative into rotation period and its respective derivative. I did so with the simple relation:

$$P = \frac{1}{f} \text{ and } \dot{P} = \frac{\dot{f}}{f^2}$$

Then I was able to calculate the characteristic age ( $\tau_c$ ) of each pulsar as

$$\tau_c = P/2\dot{P}$$

The surface magnetic field ( $B_0$ ) of each pulsar as

$$B = 3.2 \times 10^{19} \sqrt{P\dot{P}}$$

The spin-down energy ( $\dot{E}$ ), or the rate of energy loss as the pulsar continuously produces emission, as

$$\dot{E} = 4\pi^2 I \dot{P}/P^3$$

where  $I$  is the moment of inertia of the neutron star, this is generally assumed to be  $10^{45}$  g cm<sup>2</sup> (Lorimer & Kramer (2004)).

## 2.2 Polarimetry and Geometry

In order to analyze the polarization of these same pulsars, I conducted single-pulse polarimetric observations on the featured pulsars using Arecibo Observatory in Puerto Rico. The Arecibo observations were carried out at both P band (327 MHz) and L band (1400 MHz) using total bandwidths of 50 MHz and typically 250 MHz, respectively. The observations were then processed by Professor Rankin to provide pulse sequences that were used both to compute average polarization profiles and fluctuation spectra.

I then used a program written by Joanna Rankin, *newstkshist*, to plot the average profile of the pulsar, the Stokes parameters, and the angle of polarization traverse. Stokes parameters are calculated values that describe linear and circular polarization.

This then allowed me to measure the profile widths and the arc of polarization traverse across the pulse.

*Newstkhist* provided values for total intensity of the pulse, as well as a  $3\sigma$  error estimation, and I was able to use this to calculate the flux of each pulsar along with its corresponding uncertainty.

The longitude-resolved fluctuation (lrf) spectra of the pulse sequences (e.g., see Deshpande & Rankin 2001) were computed in an effort to identify subpulse “drift” or stationary modulation associated with a rotating (conal) sub-beam system. They show quasi-periodic behavior, and frequency of the occurrence.

Additionally, we attempted to calculate the height of emission for each pulsar, the angular offset of the magnetic axis from the rotation axis  $\alpha$ , the angle between the magnetic axis and the line of sight  $\beta$ , and the curvature of radiation  $\rho$ . Profile widths are measured for outer conal components and where possible estimated for cores. Core widths can be used to estimate  $\alpha$ . PPA-traverse central rate  $R$  can then be used to estimate  $\beta$ . The conal widths are used to estimate the curvature of radiation  $\rho$  using the following formulas:

$$W_{core} = \frac{2.45^\circ \sqrt{P}}{\sin \alpha}$$

$$R = \sin \alpha / \sin \beta$$

$$\rho = \arccos(\cos(\beta) - 2\sin(\alpha)\sin(\zeta)\sin^2(\Delta\psi/4))$$

$$h = \rho \frac{2.45}{\sqrt{P}}$$

Where  $W_{core}$  is the estimated width of the core of emission,  $\Delta\psi$  is the overall profile width,  $P$  is the pulse period,  $\zeta$  is the angle between the rotation axis and the line

of sight, and  $R$  is the slope of the linear polarization sweep. These equations come from Rankin (1993).

### **2.3 B0329+54**

For the mode switching work, we use uncalibrated archival data obtained from the Effelsburg Radio Telescope at 8300, 5000, 2700, and 1400 MHz. We used a code (very kindly) provided by Ramesh Karuppusamy of the Max Planck Institute fur Radioastronomie to convert the files from EPOS—or the format created by the Effelsburg Telescope—to ascii. Then, I wrote a program in Fortran 77 to average each of the four channels in order to find the calibration height given at the beginning of each file. At the beginning of each pulse, the telescope gives the calibration signal so that differences in temperature of the machine do not interfere with the recorded intensity of the pulses: otherwise, it may appear as though some pulses are much stronger than others, or some channels, when it was simply an amplification effect of the machine. We subtracted the calibration height from the un-averaged channels, and were then able to create the Stokes parameters.

From here, I used Professor Rankin’s Newstkshist program to create profiles that show pulse intensity along with the Stokes parameters. I measured the relative heights of the three components in order to quantify the difference between modes. I used a code written by Professor Mitra in order to create identical plots to their 2007 paper showing arc of polarization across the pulse and was able to calculate the values relating to its RVM solution (using values output from the program).

I then measured the pulse longitude where the angle of linear polarization was 0, and compared that with longitude of the center of the profile. This difference in longitude  $\Delta\phi$  is an effect of the height of emission, called abberation/retardation, and can allow us to calculate the height of emission by the following formula:

$$r = \frac{c\Delta\phi P}{4*360}$$

Where P is the pulse period.

And lastly, I divided the pulses up (into 5 equal groups) based on intensity and plotted the lowest group against the highest. An affect of abberation/retardation is to throw the higher intensity pulses forward by a small amount, but only in the core emission. If the core component is abberated/retarded by the same amount in each mode, it is an additional confirmation that the height of the emission has not changed, and the emission process for the core has also remained the same.

## 3 Data Analysis

### 3.1 Timing

The characteristics of the timing observations are given in Table 1, together with the number of pulses—here called Times of Arrival or TOA’s—derived for each, the root mean square (rms) of the residuals, and the reduced  $\chi^2$  of each fit.

For some pulsars,  $\chi^2$  is much larger than 1, implying the presence of timing noise due to factors that were not taken into account and corrected for. This is more

Previous Name	Reference	New Name	Start (MJD)	Finish (MJD)	Epoch (MJD)	N	rms (ms)	$\chi^2$
J0435+27	Ray et al. (1996)	J0435+2749	52854	53785	53400	96	0.12	5.83
J0517+22	Chandler (2003)	J0517+2212	53418	53774	53400	98	0.11	2.07
J0627+07	Chandler (2003)	J0627+0706	53418	53675	53400	91	0.26	13.71
J0927+23	Ray et al. (1996)	J0927+2345	53318	53858	50000	23	0.47	1.59
J0943+22	Thorsett et al. (1993)	J0943+2253	53318	53910	50000	83	0.20	1.80
J0947+27	Ray et al. (1996)	J0947+2740	53318	53910	50000	35	0.28	1.88
J1246+22	Thorsett et al. (1993)	J1246+2253	53294	53672	53294	88	0.24	1.61
J1404+12	Chandler (2003)	J1404+1159	53309	53672	50000	66	0.37	1.98
J1756+18	(Navarro et al., 2003)	J1756+1822	52645	53307	52751	89	1.23	2.90
J1935+12	Chandler (2003)	J1935+1159	53306	53580	53295	40	2.43	0.70
J2050+13	(Navarro et al., 2003)	J2050+1259	52636	53306	52773	27	8.81	6.31
J2052+17	Thorsett et al. (1993)	J2053+1718	53295	56837	55000	728	0.028	1.34

Table 1 lists the pulsar’s name as determined by previous surveys, the citation for the original discovery, and the new name as determined by our observations. Also provided is the start, end, and reference epochs in modified Julian dates, the number of pulses recorded, the rotation measure, and reduced  $\chi^2$  for the timing solutions.

prominent for the younger pulsars in this work, in particular for J0627+0706, due to the fact that younger pulsars often have more turbulence than older more stable pulsars. The table also gives the new names for these pulsars (most notably now with four digits of precision for the declination). The best fit values for Right Ascension  $\alpha$  and Declination  $\delta$  are presented in Table 2, together with the other numerical parameters of the timing solution such the rotation frequency ( $\nu$ ), its derivative ( $\dot{\nu}$ ) and dispersion measure (DM).

Finally, the derived parameters are given in Table 3: Galactic coordinates ( $l, b$ ) and distance ( $D$ ), derived from the previous 3 quantities using the NE 2001 model of the electron distribution of the Galaxy (Cordes & Lazio, 2002), spin period ( $P$ ) and its period derivative ( $\dot{P}$ ), The expressions for these quantities were adopted from Lorimer & Kramer (2004), as listed earlier. All pulsars in the list are isolated, and most of them belong to the “normal” group, with fairly typical rotation periods

Table 2. Timing Parameters

Pulsar Name	RA	Dec	$\nu$ (Hz)	$\dot{\nu}$ ( $10^{-16}$ Hz s $^{-1}$ )	DM (pc cm $^{-3}$ )
J0435+2749	04 35 51.8178(16)	27 49 1.68(16)	3.06457408039(5)	-0.767(4)	53.192(9)
J0517+2212	05 17 17.159(7)(72)	22 12 48.8(1.6)	4.9707996302(9)	-2.20(6)	18.691(9)
J0627+0706	06 27 44.2168(15)	07 06 12.67(29)	2.10139608235(13)	-1314.82(11)	138.289900
J0927+2345	09 27 45.26(4)	23 45 11.(1)	1.3125269006(16)	-5.26(5)	17.24(10)
J0943+2253	09 43 32.403(5)	22 53 5.98(11)	1.87626174158(26)	-3.168(8)	27.209(17)
J0947+2740	09 47 21.287(13)	27 40 43.48(18)	1.1750682463(7)	-5.937(21)	29.09(5)
J1246+2253	12 46 49.3610(28)	22 53 43.12(10)	2.11028093179(6)	-3.89(4)	17.793(22)
J1404+1159	14 04 36.961(8)	11 59 14.4(3)	0.3772960811(6)	-1.893(18)	18.530(27)
J1756+1822	17 56 17.582(5)	18 22 55.26(13)	1.34408437573(3)	-9.266(17)	70.800000
J1935+1159	19 35 15.87(23)	11 59 6.(54)	0.5155281800(14)	-2.7(11)	191.6(26)
J2050+1259	20 50 57.21(5)	12 59 9.69(14)	0.81898743453(12)	-3.38(6)	52.400000
J2053+1718	20 53 49.4806(4)	17 18 44.692(7)	8.384495640456(4)	-0.002014(7)	26.979

Table 2 lists the precise right ascension and declination values as recorded from the timing observations. We give the frequency, frequency derivative, and dispersion measure, as determined from the timing observations.

Table 3. Derived Parameters

Pulsar Name	Galactic Coordinates		$P$	$\dot{P}$	$\tau_c$	$B_0$	$D$	$\dot{E}$
	$\ell$	$b$	(s)	( $10^{-15}$ s s $^{-1}$ )	( $10^9$ yr)	( $10^{12}$ G)	(kpc)	( $10^{24}$ W)
J0435+2749	171 50 32.0	-13 04 17.3	0.326279534509(6)	0.00816(5)	0.63	0.052	1.8	0.927
J0517+2212	182 10 37.1	-09 00 46.0	0.222366515211(5)	0.01087(28)	0.32	0.050	0.66	3.899
J0627+0706	203 54 25.4	-01 59 35.5	0.47587411455(3)	29.7748(24)	0.00025	3.81	4.7	1090
J0927+2345	205 17 09.1	+44 12 05.6	0.7618891464(9)	0.3051(28)	0.040	0.49	0.66	2.723
J0943+2253	207 53 11.5	+47 27 29.9	0.53297467930(7)	0.09000(23)	0.094	0.22	1.2	2.347
J0947+2740	201 08 31.0	+49 23 04.2	0.8510136770(5)	0.4300(15)	0.031	0.61	1.28	2.754
J1246+2253	288 48 32.7	+85 38 23.7	0.473870556729(13)	0.0874(8)	0.086	0.21	1.5	3.242
J1404+1159	355 04 37.3	+67 06 51.9	2.650438343(4)	1.330(13)	0.032	1.90	1.4	0.282
J1756+1822	43 50 08.5	+20 11 07.1	0.744000910999(17)	0.5129(9)	0.023	0.63	4.2	4.917
J1935+1159	48 36 43.9	-04 03 31.7	1.939758172(5)	1.0(4)	0.031	1.41	6.8	0.541
J2050+1259	59 26 11.6	-19 14 21.3	1.22101995445(17)	0.504(9)	0.038	0.79	3.1	1.093
J2053+1718	63.5541	-17.2643	0.11926775835804(5)	0.0002864(10)	6.7	0.0058	1.9	0.65

Table 3 lists the parameters calculated using the timing solutions. We've calculated the galactic coordinates from the right ascension and declination values listed in Table 2. The period and period derivative from the frequency and frequency derivative in Table 2. The age of the pulsar ( $\tau$ ), the magnetic field ( $B_0$ ) and the energy loss rate ( $\dot{E}$ ) were then calculated from the period and period derivative. The distance to the pulsar was calculated using the dispersion measure.

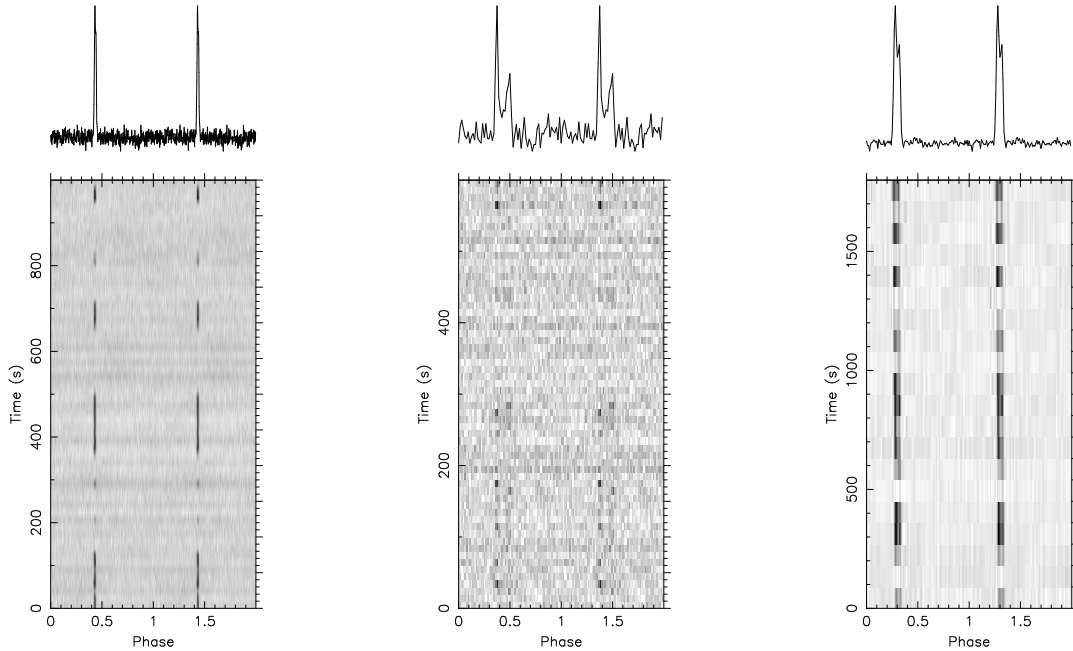


Figure 1: Single-pulse sequences that show nulling for J0943+2253, J1935+1159 and J2050+1259

(between 0.22 and 2.65 s), characteristic ages (between 0.25 Myr and 0.63 Gyr) and B-fields (from 0.05 to  $3.8 \times 10^{12}$  G).

When plotted as single pulses, three pulsars showed nulling behavior as shown in Figure 1. Pulsar nulling is when the emission we see stops for a period of time—ranging from a few seconds up to years—but then turns back on right where it left off. There are numerous efforts to theorize why pulsars do this, yet the problem remains largely unsolved.

The timing of J2053+1718 yields some interesting results, in addition to demonstrating that it is indeed a pulsar. It has a spin period of 119 ms, a relatively low

magnetic field of  $5.810^9$  G and a characteristic age of 6.9 Gyr; this suggest the pulsar was mildly recycled by accretion from a companion star because it spins incredibly fast for a pulsar of its age and magnetic field strength. The fact that it is now isolated suggests it was a member of a proto-double neutron star system, which never formed because the system became unbound when the secondary star in the system became a supernova.

## 3.2 Polarimetry and Quantitative Geometry

A summary of the polarimetric observation details are given in Table 4, as well as flux estimates and Rotation Measure (or RM). Values for the RM were calculated by Professor Joanna Rankin , and a complete description of the methods and errors will be given in Rankin, Venkataraman & Weisberg (2017).

Below I will analyze the various pulsars individually, referring to the polarized profiles and fluctuation spectra in the Appendix figures. The analyses proceed from polarimetry and fluctuation spectra to quantitative geometry.

### 3.2.1 Polarimetry and Fluctuation-spectral Analysis

**J0435+2749** has a clear triple profile at both frequencies as shown in Figure A1, though the L-band profile is of better quality. The leading and trailing components have very different spectral indices: the trailing component is much stronger at 327 MHz, but the leading is much stronger at 1400 MHz. The fractional linear polariza-

Name	MJD		Pulses		Flux Estimates (mJy)		RM (rad-m <sup>2</sup> )
	P-band	L-Band	P-band	L-Band	P-Band	L-Band	
J0435+2749	53490	54541	1840	3065	1.9(6) $\times 10^{-7}$	0.24(3)	+2
J0517+2212	57123	54540	2696	2698	119.(8)	0.52(2)	-16
J0627+0706	57123	57113	518	2520	8(5)0	0.25(4)	+212
J0927+2345	57525	57347	4724	2502	1.9(8)	0.02(2)	-8
J0943+2253	57379		7775		5.3(1)		+8?
J0947+2740	57379	57524	3172	4699	8.8(1)	0.027(9)	+32
J1246+2253	52840	57307	1266	1885	—	0.21(9)	+4?
J1404+1159	55905	57307	509	1591	68.(8)	<0.01	+4
J1756+1822	57567	57567	2156	3571	<0.008	<0.05	+70
J1935+1159	57288	57533	1004	1090	<10	0.47(5)	-83
J2050+1259	57524	57525	2046	1966	10.(4)	0.025(8)	-80
J2053+1718	57524	57533	5023	21624	<19	<0.0006	-5

This table gives the modified Julian dates of our polarimetric observations at each band, their length in pulses, flux density estimates and corresponding  $3\sigma$  errors, and the nominal rotation-measure values used.

tion is low in both profiles such that the polarization-angle traverse is well defined only at the higher frequency. The power under the leading component may represent a different orthogonal polarization mode (OPM) than the remainder, suggesting little polarization position angle (PPA) rotation across the profile. Both fluctuation spectra show broad peaks at about 0.05 cycles/period, primarily in the two outer components, which suggest a 20-period conal modulation.

**J0517+2212** has a double component profile at L-band, whereas its P-band profile shows some structure in the second component. The polarization traverse shows little rotation at P band apart from the two  $90^\circ$  “jumps” and the behavior seems similar at L band but less well resolved, perhaps because of the diminished fractional linear polarization. The fluctuation spectra show a peak around 0.12 cycles/period, suggesting an 8 rotation-period modulation.

**J0627+0706** has a bright interpulse, a component-peak separation of  $177^\circ$  (main

pulse minus interpulse peak longitudes) as can be seen in Fig. 6. Because both features have structure, more detailed interpretation is needed to assess how close to  $180^\circ$  they fall; however, given the narrowness of both features, it seems likely that they represent emission from the stars two poles, implying an orthogonal geometry where  $\alpha$  is close to  $90^\circ$ . PPA tracks give hints about the geometry only at L band, and here little to go on apart from a probable  $90^\circ$  “jump” under the main pulse. The main pulse might have three components and the interpulse two. The fluctuation spectra are not displayed because they showed only flat “white” fluctuations.

**J0927+2345** shows an interesting feature at P-band approximately  $180^\circ$  away from the main pulse (Fig. A4) . This apparent interpulse is discernible only in the P-band profile, and disappears in the L-band one. Again both profiles show so little linear polarization that a reliable PPA rate can be estimated for only a narrow longitude interval at P band. The main pulse appears to have three closely spaced features. Again the fluctuation spectra are not given because they showed no discernible features.

**J0943+2253** nulls as seen in Fig. 1 above, but the fluctuation spectra show no quasiperiodic behavior. The polarization is slight and the PPA track shows what appears to be a  $90^\circ$  “jump” within the narrow interval where it is clearly defined.

**J0947+2740** shows three components at both frequencies, though the leading region may be more complex at the lower frequency, probably representing a core and closely spaced inner cone. At L-band the conal components are weaker, and the PPA traverse is more complex, perhaps showing a  $90^\circ$  “jump” in the region of rapid PPA rotation.

RVM behavior, and the slope of its polarization traverse, could not be determined. This pulsar is also known to exhibit sporadic emission between intervals of weakness or nulls as in Fig. 1. The fluctuation spectra seem to hint at fluctuation power at periods longer than about 3 or 4 pulses (apart from the RFI features in the P-band plot).

**J1246+2253** has a single component at P band, which develops into a resolved triple form at L band in what may be the characteristic core-single manner. The fractional linear polarization at both frequencies is low, so little can be discerned reliably from the PPA tracks. Also no clear features are seen in the fluctuation spectra as is often the case for core-single profiles.

**J1404+1159** exhibits a narrow peak in its fluctuation spectra around 0.2 cycles/period, suggesting a modulation period  $P_3$  of some 5 rotation periods. A display of its individual pulses bears this out, and a display of its emission folded at  $P_3$  shows that the modulation is highly regular. The PPA rate at the profile center suggests an outside sightline traverse as is usual for conal single “drifters”. See Figure 6.

**J1756+1822** appears to have two profile components, and its profile broadens perceptibly with wavelength suggestion a conal double configuration. The P-band polarization is negligible, whereas a hint of a moderately steep negative PPA traverse is seen at L-band. The fluctuation spectra showed no features and were thus omitted.

**J1935+1159**’s long nulls (see Fig. 1) make this pulsar difficult to observe sensitively, and neither clear profile structure or polarization signature is seen at either frequency.

Similarly, fluctuation spectra showed nothing useful.

**J2050+1259** also exhibits frequent nulls as seen above in Fig. 1. However, its single profile at L band broadens and bifurcates at P band in the usual conal double manner, and a steep PPA traverse is seen at the lower frequency. Finally, here we do see strong low frequency features in the fluctuation spectra indicative of modulation on a scale of 50 rotation periods or longer.

**J2053+1718** Our P and L band observations do not provide much polarization information or fluctuation-spectral information apart from it having a single profile at both frequencies.

### 3.2.2 Quantitative Geometry

We have also attempted to classify the profiles where possible and conduct a quantitative geometrical analysis following the procedures of the core/double-cone model in Rankin (1993a,b; hereafter ETVI). The notes to Table 5 summarize our measurements, and the table values show the results of the geometrical model for the pulsar's emission beams. The profiles class is given in the first column,  $\alpha$  and  $\beta$  in next two per the  $R$  value when possible. The conal component profile widths  $w$ , conal beam radii  $\rho$ , and characteristic emission heights  $h$  are tabulated in the rightmost three columns.

**J0435+2749**'s average profile has a triple component configuration at both frequencies, and the observed conal spreading suggests a core/outer cone geometry. The core width can only be estimated at the higher frequency at perhaps  $9^\circ$  maximum, im-

Table 5. Conal Geometry Models						
Pulsar	Class	$\alpha$ ( $^\circ$ )	$\beta$ ( $^\circ$ )	$w$ ( $^\circ$ )	$\rho$ ( $^\circ$ )	$h$ (km)
J0435+2749	T	18	3.4	59.0	10.3	230
J0517+2212	D	31	0	45.2	11.7	205
J0627+0706m	$S_t$	90	-7.2	4.54	7.5	131
J0627+0706i	D	90	-6.4	6	6.9	129
J0927+2345m	D/T?	69	3.4	8	5.1	130
J0943+2253	D/T?	42	-5.5	7	5.9	123
J0947+2740	T/M	42	-1.2	18	6.0	205
J1246+2253	$S_t$	81	-4.7	6.5	5.7	103
J1404+1159	$S_d$	25	2.2	5.3	0.88	114
J1756+1822	D	50	2.5	16	6.7	224
J1935+1159	D	10.13	-1.0	50.4	4.3	239
J2050+1259	$S_d$	27	-2.6	21	5.2	223
J2053+1718	$S_t?$	63	-17.2	2.5	17.2	235

Notes: outer half-power widths interpolated to 1 GHz above:

*J0435+2749*:  $63^\circ$  at P-band and  $59^\circ$  at L-band;  $R \sim 5^\circ/^\circ$ .

*J0517+2212*: The profile narrows from  $55^\circ$  at P-band to  $45.5^\circ$  at L-band. There was a similar angle of polarization angle traverse at both frequencies. I suggest central traverse, beta about 0

*J0627+0706*: The main pulse measures approximately  $4.5^\circ$  at both L-band and P-band at half maximum, while the interpulse is wider at half maximum measuring  $6^\circ$ . The main pulse and the interpulse are  $178^\circ$  apart.

*J0927+2345*:  $5^\circ$  at P-band and  $6.4^\circ$  at L-band.

*J0943+2253*: This pulsar has width  $6.5^\circ$  at P-band half max. The core widths are measured as  $12^\circ$  at L-band and  $15.6^\circ$  at P-band. The PPA slope was measured at P-band.

*J0947+2740*: Outside 3-db widths of  $19.4^\circ$  at P-band and  $17^\circ$  at L-band; central component widths of roughly  $8^\circ$  at P-band and  $10^\circ$  at L-band;  $R \sim 32^\circ/^\circ$ .

*J1246+2253*  $5.7^\circ$  at P-band and  $7.4^\circ$  at L-band interpolated to  $6.5^\circ$  at 1 GHz above;  $R \sim +12^\circ/^\circ$ .

*J1404+1159*:  $R \sim 11$ . This pulsar has width  $5.8^\circ$  at P-band and  $5.0^\circ$  at L-band.

*J1756+1822* This pulsar has estimated core widths  $8.2^\circ$  at P-band and  $7.1^\circ$  at L-band, with total profile widths of  $16^\circ$  at P-band and  $15.3^\circ$  at L-band. The PPA traverse was measured using L-band data.  $\sim 16^\circ$  at P-band and  $15^\circ$  at L-band;  $R \sim -18^\circ/^\circ$ .

*J1935+1159*: This pulsar has width  $51.8^\circ$  at P-band and  $50.5^\circ$  at L-band.

*J2050+1259* widths  $\sim 25^\circ$  at P-band and  $18^\circ$  at L-band. Despite very weak polarization across the pulse, we've estimated the polarization angle traverse as  $10^\circ/^\circ$  at P band where there is a clear signature.

*J2053+1718*: This pulsar has width  $2.497^\circ$  at P-band and  $5^\circ$  at L-band.

plying that  $\alpha$  is less than  $1.4^\circ$ .

The PPA traverse shows a much more complex behavior than the Rotation Vector Model (RVM) describes; however, the roughly  $90^\circ$  rotation near the center of the pulse may be so interpreted. The spherical geometric beam model in Table 5 seems compatible with a core-cone triple **T** classification.

**J0517+2212**'s profile shows two primary components. There is more structure at L-band, as well as overall pulse narrowing. These factors, along with the confused PPA traverse leave little recourse but to assume  $\beta \sim 0$ , which in turn suggests the outer conal beam geometry shown in Table 5.

**J0627+0706**'s main-pulse profile may have two or three closely spaced components. The pulse width at half maximum interestingly widens from P-band to L-band suggesting a core-single configuration where the conal emission is seen mainly at high frequency. The polarization traverse is clearer at L-band, marked by prominent  $90^\circ$  modal “jumps”. It thus seems likely that  $\beta$  is small for the main pulse and perhaps larger for the inter pulse, but that  $\alpha$  is close to  $90^\circ$ , yielding the classifications and model values in Table 5. The emission heights given for both the main pulse and interpulse suggest that it is inner conal emission.

**J0927+2345**'s average profile has two clear components and possibly an unresolved trailing one as well. Its half width interestingly broadens from P-band to L-band suggesting a core single evolution where conal “outriders” appear or become more prominent at high frequency. The polarization traverse is well defined only for short interval at L band, and this may provide a useful  $R$  value, leading to the geometric

beam model in Table 5. If this profile were triple, the central component would be  $2.8^\circ$  wide.

**J0943+2253**'s average profile also has two closely spaced components and perhaps an unresolved weak feature on its leading edge, suggesting a double or triple configuration. We only have a P-band observation so cannot see how the profile evolves, and the linear polarization is slight and difficult to interpret. However, we can guess a central PPA rate of  $7^\circ/\circ$  in order to compute the geometric model parameters in Table 5, which suggest an inner-conal configuration.

**J0947+2740**'s profile is comprised of three main components, and its width increases with wavelength. This indicates an outer-conal configuration. Its PPA traverse seems interpretable per the RVM model at P band, but its L-band traverse seems to be distorted by what may be a  $90^\circ$  “jump” just prior to the profile center. Its profile then seems to be a core/outer cone triple, and the quantitative beam geometry model is shown in Table 5. The core width is estimated around  $2.65^\circ$ , which is much more narrow than the central component of the profile ( $7.92^\circ$  at P-band and  $10.08^\circ$  at L-band), which indicates that the central component contains both core and conal emission.

**J1246+2253**'s single profile at P band becoming triple at L band strongly suggests a core single configuration. Despite the low fractional linear polarization, the trailing positive traverse through roughly  $90^\circ$  was used to computer the geometrical model in Table 5. The core width is estimated at  $3.55^\circ$ .

**J1404+1159** has a single component profile at both frequencies, and its narrow

fluctuation feature identifies it as having regular drifting subpulses as shown in Fig. 6. The pulsar then appears to have a classic conal single profile. Both PPA tracks show a negative-going traverse with a central slope of about  $-12^\circ/^\circ$ . Here we also give short pulse-sequences folded at the modulation period of some 0.2 rotation-periods/cycle.

**J1756+1822** has an interestingly shaped profile that appears to have two separate components. The P and L-band profiles have similar forms with the longer wavelength one somewhat broader in the usual pattern of the conal double class. The fractional linear profiles is low at both frequencies, but at L-band there seems to be a hint of a traverse through more than  $90^\circ$  across the profile. The fluctuation spectra are not shown as no features could be discerned.

**J1935+1159**'s filled profile suggests three- or five-component core-cone structure. Conal double profiles do not usually show such forms. Measurements show that the profile is narrowing from P-band to L-band, and the geometry in Table 5 suggests an outer cone which is filled with inner conal and/or core emission. For the geometric computations, we have estimated a central traverse of  $10^\circ/^\circ$ .

**J2050+1259**'s profile has a single component at Lband and two closely spaced components at P band as seen in Fig A11. Its profile is broader at the lower frequency, and strong hints of a roughly  $180^\circ$  PPA traverse are seen in both profiles, suggesting that this is a conal single profile with a small impact angle with the beaming parameters as given in Table 5.

**J2053+1718** shows a single component at both frequencies, though in the higher

Frequency MHz	MJD	Number of Pulses in Each Mode		Total Profile Width	
		Normal	Abnormal	Normal	Abnormal
1400	51971	1-1000	1,000-3,000	23.4°	22.5°
8300	53184	1-2700	2700-3000	23.2°	22.0°

frequency observation the time resolution was poor with only 232 samples across the rotation cycle. Neither the polarization information nor the fluctuation spectra give much to go on. Curiously, this pulsar has a wider profile in L-band than in P-band, however much of this can probably be attributed to the quality of the observation. Its short 119-ms rotation period and single profile do suggest a core-single classification.

### 3.3 B0329+54

We found mode switching in data from 1400 MHz as well as 8300 MHz. The mode change is characterized by the intensity of the third component relative to the first two components: at lower frequencies (300 MHz-1400 MHz) the third component shrinks, while at higher frequencies (8300 MHz) it grows. By looking at average profiles, we can see that at 1400 MHz the third component shrinks from 28 percent the strength of the main pulse, to about 19 percent the strength. At 8300 MHz, the third component grows from 33 percent of the main pulse strength to 122 percent. These images are shown in Figure 2.

The mode switching occurs within a pulse period (0.714s), and can remain stably in the abnormal mode for up to thousands of pulses. This indicates that whatever

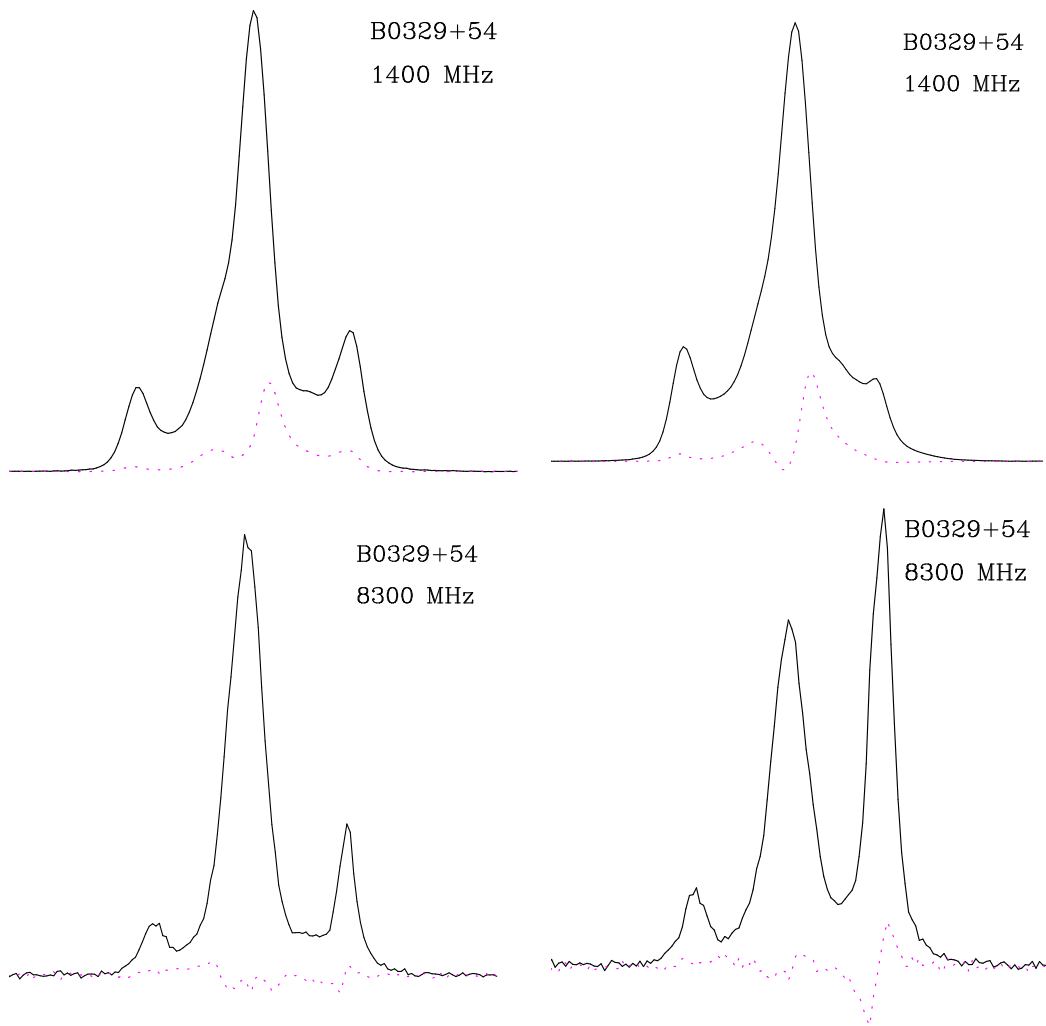


Figure 2: The profile shape appears quite different for the abnormal mode at different frequencies. Across the top: the normal mode is given on the left, with the abnormal on the right at 1400 MHz. Across the bottom: the normal is given on the left, with the abnormal mode on the right at 8300 MHz.

mechanism is responsible for switching modes must operate on a nearly instantaneous timescale.

The profiles appear more differentiated between frequencies in the abnormal mode, and the profile shapes that we have identified as normal and abnormal correspond closely with those identified by Bartel et al.

### 3.3.1 Polarization Properties of B0329+54 at 1400 MHz

We investigated the single pulse polarization properties for both modes. First, we separated pulses based on intensity, grouping them into five groups. We found that there was virtually no change with the polarization position angle traverse between the two modes, as shown in the right hand side of Fig 3. At higher intensity pulses, a non-RVM kink emerges: the polarization angle changes more rapidly across the central component.

In a similar method to Mitra et al, we found that the lowest intensity pulses follow the rotation vector model  $\chi = \tan^{-1} \frac{\sin(\alpha)\sin(\phi)}{\sin(\alpha+\beta)\cos(\alpha) - \sin(\alpha)\cos(\alpha+\beta)\cos(\phi)}$  with identical parameters ( $\alpha = -35.5^\circ$ ,  $\beta = 3.7^\circ$ , and  $\phi = -25.3^\circ$ ) in each mode. Therefore, there's very little difference between the polarization behavior in the core component of the emission.

We also took a closer look at each of the Stokes parameters, and have compared them between the normal and abnormal mode. We present overlaid comparisons in Figure 4, showing the total intensity  $I$ , the total linear polarization  $L = \sqrt{Q^2 + U^2}$ , the total circular polarization  $V$ , and the polarization position angle. We see that

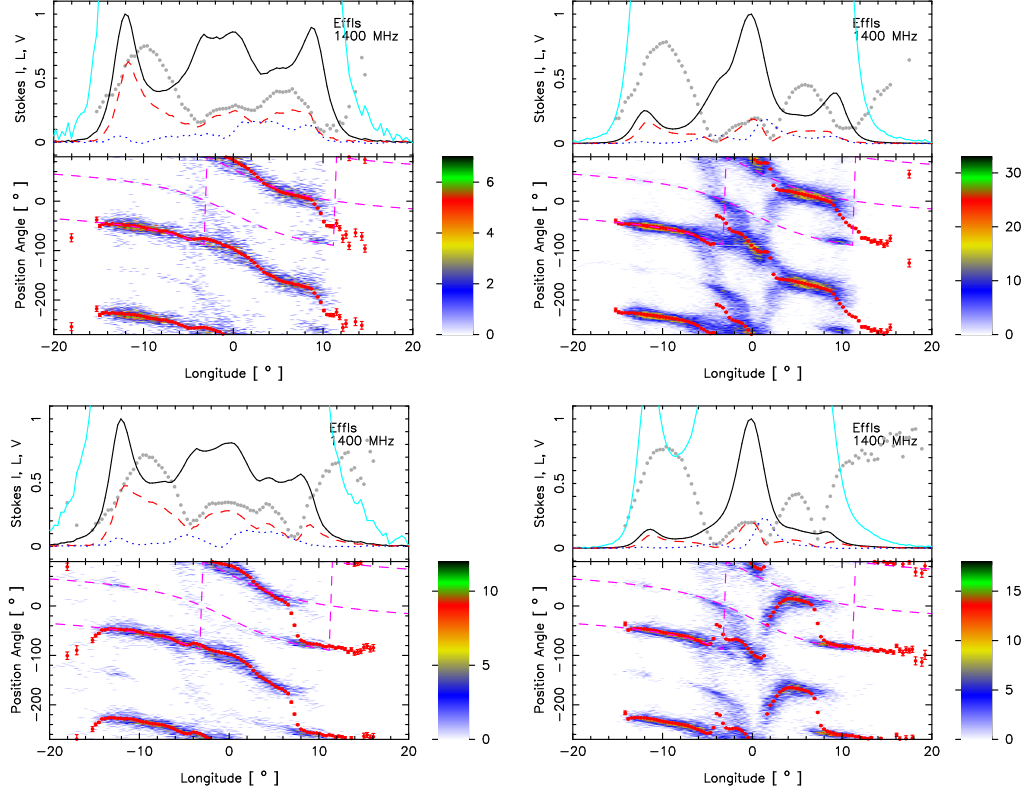


Figure 3: The four images show the linear polarization angle across the pulse. The top two images show the normal mode, while the bottom two show the abnormal mode. The images on the left show low intensity pulses with RVM polarization, while the images on the right show high intensity pulses with the polarization angle kink. The total power Stokes I, linear polarization L, and circular polarization V are given in the respective top panels, and the polarization-angle [ $\chi = (1/2)\tan^{-1}(U/Q)$ ] density is plotted using color scale in the central panels.

the overall width of the profile remains constant between modes, and overall profile shape remains constant (save the proportional shrink of the third component). Both linear and circular polarization remain very similar throughout the first and central component, but differ in the third. For linear polarization, there is a large dip in the third component—showing up as a bifurcated feature. Correspondingly, in the graph of polarization position angle, we see a sharp change in the PPA at the same longitude as we see the linear polarization dip. We also do not see a strong circular polarization presence in the third component of the abnormal mode, while we do see so in the normal mode third component.

### 3.3.2 Geometry and Emission Heights

Since we have identified the polarization properties as nearly identical between the two modes, the next property to compare is the height of emission. If we can show that the height remains constant between modes, it will further constrain the cause of mode switching. The rotating vector model was applied to find the steepest gradient point for lowest intensity pulses, allowing us to calculate the emission height using aberration/retardation methods.

The longitude difference between the center of the total intensity profile and the steepest gradient of the position angle curve  $\Delta\phi$  was determined from the low intensity profiles in Figure 3. From there the height can be calculated as  $r = \frac{c\Delta\phi P}{4*360}$ . I measured the difference as  $2^\circ$  for both modes, which gives an approximate emission height of 300km for both modes.

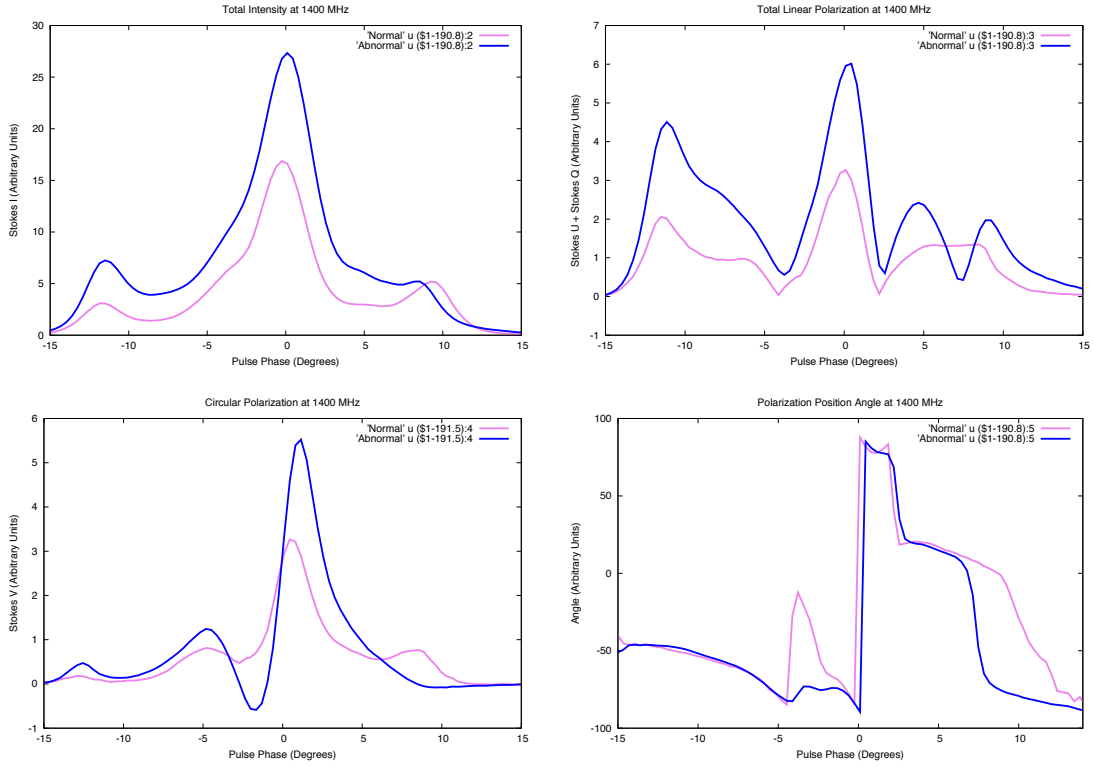


Figure 4: The four images above show a direct comparison of the intensity, linear polarization, circular polarization, and polarization position angle between the modes. The Normal mode data is given in violet while the abnormal mode data is given in dark blue.

Lastly, the difference in profile center at different intensity groupings for both modes are shown in figure 5. The center of the maximum intensity pulses was found to shift by  $2^\circ$  also at both frequencies, further highlighting no change in emission height or core component emission mechanism.

## 4 Results and Discussion

The emission from both modes follows the same RVM solution for low intensity pulses, and exhibits the same PPA “kink” for high intensity pulses. This means that nothing about the overall emission mechanism or dipolar magnetic configuration changes between modes, and therefore cannot be responsible for mode switching. Additionally, the emission is generated at the same height above the pulsar in each mode, so differences in height cannot be responsible for mode switching.

The following formula determines the frequency of radio emission  $\omega$  produced by curvature radiation:

$$\omega = \frac{3c}{2\rho}\gamma^3$$

Where  $\gamma$  is the Lorentz factor for the accelerated electrons, and  $\rho$  is the curvature of radiation, which is directly related to the emission height.

The power of emission produced is therefore:

$$P = \frac{2c}{3\rho^2}\gamma^4Q^2$$

The power of the emission changes in the third component of the pulse as the mode

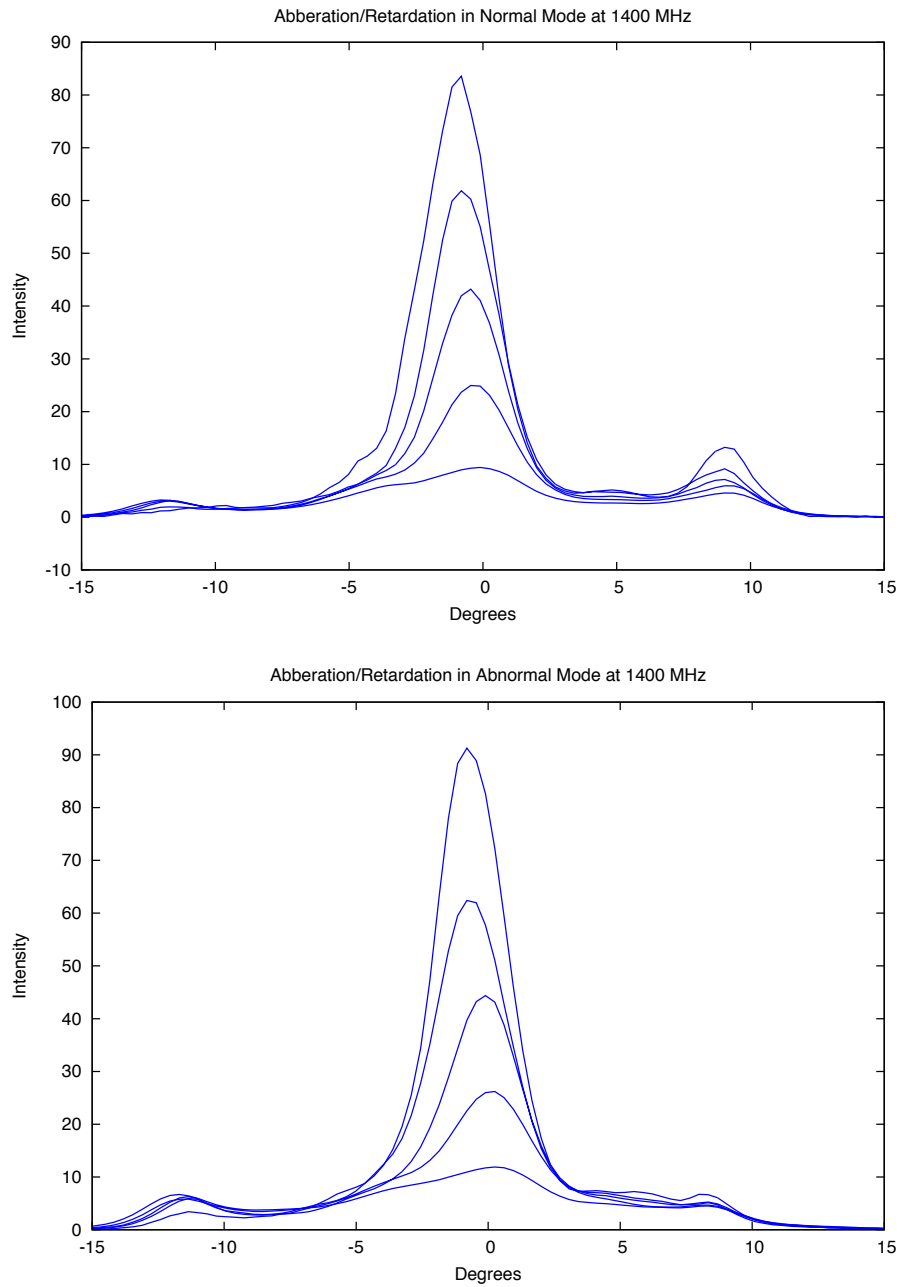


Figure 5: Normal vs Abnormal Mode Abberation/Retardation at 1400 MHz. The pulses are separated into 5 different groups based on intensity and plotted superimposed so that the angular difference between the highest intensity and lowest intensity pulses can bet seen and measured as  $2^\circ$

switches, therefore some element in the equation for power must change. We've determined that the emission height does not change between modes because the difference between the central profile longitude and the longitude of the steepest gradient of PPA traverse remains the same, therefore  $\rho$  has to remain constant. The frequency of the emission  $\omega$  remains constant between mode switches as well, therefore there can be no change in  $\gamma$ . Instead, what needs to change is the amount of charge  $Q$  available in the plasma to produce the radiation.

At 1400 MHz, the third component is at 28% the power of the central component in the normal mode, and 19% the power of the central component in the normal mode. That means the ratio of power is:

$$\frac{\sqrt{P_N}}{\sqrt{P_A}} = \frac{Q_N}{Q_A} = \frac{5.29}{4.36} = 1.21$$

This means that there needs to be a roughly 20% increase in the amount of charge  $Q$  as the pulsar switches from the abnormal mode to the normal mode.

We can also see this through the change in linear polarization between the two modes. Linear polarization is composed of two orthogonal components that both travel through the electron plasma along the magnetic field lines. Changes in charge between the two modes would decrease one component of linear polarization while not affecting the other, producing an overall change in the amount of linear polarization as well as the position angle.

The amount of charge available to produce emission comes from a cascade of electrons, where electrons and positrons are pair produced. Changes in the amount of pair production in the plasma can result in differences in profile shape without alter-

ing the emission height. In this model, a potential gap forms on the magnetic polar cap that gets discharged by pair production. As this discharge proceeds around the magnetic axis, it changes the electrostatic conditions in the sparking zone. If a source could provide additional photons at the very beginning of this process in a quasi-periodic fashion, these metastable plasma modes could produce very distinguished and regular differences in profile shape.

## 5 Conclusion

In the foregoing sections we have characterized a group of pulsars that had not been the target of any previous detailed studies. We determined timing solutions for all of them and explored their pulse-sequence properties and quantitative geometry. This has provided a useful basis for what defines usual and unusual pulsar behavior in a wide variety of areas. Three of them (PSRs J0943+2253, J1935+1159 and J2050+1259) have strong nulls and sporadic radio emission, several others exhibit interpulses (PSRs J0627+0706 and J0927+2345) and one shows regular drifting subpulses (J1404+1159). These measurements will be important in future, more global assessments of the emission properties of radio pulsars and studies of the neutron star population in the Galaxy.

More interestingly, however, we dove into the polarization characteristics of one pulsar, B0329+54, in order to isolate the most probable mechanism for mode switching. We found that the only change possible that could produce a difference in the power of emission in the third component is a change in the group charge  $Q$ . Further model-

ing is needed to show what produces this change along the electron cascade process. There could be several possible explanations for what could change the surface energy, therefore providing a different number of photons for pair production; but a wider survey of more profile mode switching pulsars could help illuminate what exactly causes the pair production to change.

The timing and polarimetry sections of this dissertation are assembled with some additional contributions by Paulo Friere into a paper titled *No Pulsar Left Behind: Timing Solutions, Pulse-sequence Polarimetry, and Emission Morphology for 12 Pulsars* which is currently in the submission process to the Monthly Notices of the Royal Astronomical Society. The B0329+54 sections of this dissertation are also assembled into a paper that we hope to have finished and submitted by the end of May.

## 6 Acknowledgements

There are many people I'd like to thank, and who have made this dissertation possible. First, I would like to thank Professor Joanna Rankin. As my research advisor for four years, Professor Rankin has taught me useful research skills and has added my work and my voice on to these two projects. She has introduced me to the larger world of astronomy, and I would absolutely not be where I am today without her.

Next, I would like to thank Dipanjan Mitra. He motivated me—aka forced me—to learn how to become a self-sufficient coder, and he coached me to discover the

reasons behind mode switching on my own. He has had an enormous impact on my research, my approach to learning physics, and my life in general. I would also like to thank Paulo Friere, who took me under his wing at the Max Planck Institute in Bonn.

I would like to thank Renee Beneski and Toria Ainsworth, fellow UVM physics students and dear friends, for helping me edit this dissertation so that it is readable to those who are not entrenched in the jargon of pulsars.

Finally, I would like to thank my mom Cheryl Brinkman for being my first science teacher. My mom was always ready to answer questions such as “what are stars made of” and has always fostered my love for studying the cosmos.

## References

Chandler A. M., 2003, PhD thesis, CALIFORNIA INSTITUTE OF TECHNOLOGY

Cordes J. M., Lazio T. J. W., 2002, ArXiv Astrophysics e-prints,  
<http://adsabs.harvard.edu/abs/2002astro.ph..7156C>

Lorimer D. R., Kramer M., 2004, Handbook of Pulsar Astronomy

Mitra D., Melikidze G., Gil J., 2015, in Astronomical Society of India Conference Series. (<http://arxiv.org/abs/1510.00103> arXiv:1510.00103)

Navarro J., Anderson S. B., Freire P. C., 2003, <http://dx.doi.org/10.1086/377153> ,  
<http://adsabs.harvard.edu/abs/2003ApJ...594..943N> 594, 943

Rankin J. M., 1993, <http://dx.doi.org/10.1086/172361> ,  
<http://adsabs.harvard.edu/abs/1993ApJ...405..285R> 405, 285

Ray P. S., Thorsett S. E., Jenet F. A., van Kerkwijk M. H., Kulkarni S. R.,  
Prince T. A., Sandhu J. S., Nice D. J., 1996, <http://dx.doi.org/10.1086/177934>  
, <http://adsabs.harvard.edu/abs/1996ApJ...470.1103R> 470, 1103

Thorsett S. E., Deich W. T. S., Kulkarni S. R., Navarro  
J., Vasisht G., 1993, <http://dx.doi.org/10.1086/173224> ,  
<http://adsabs.harvard.edu/abs/1993ApJ...416..182T> 416, 182

## Appendix of Images

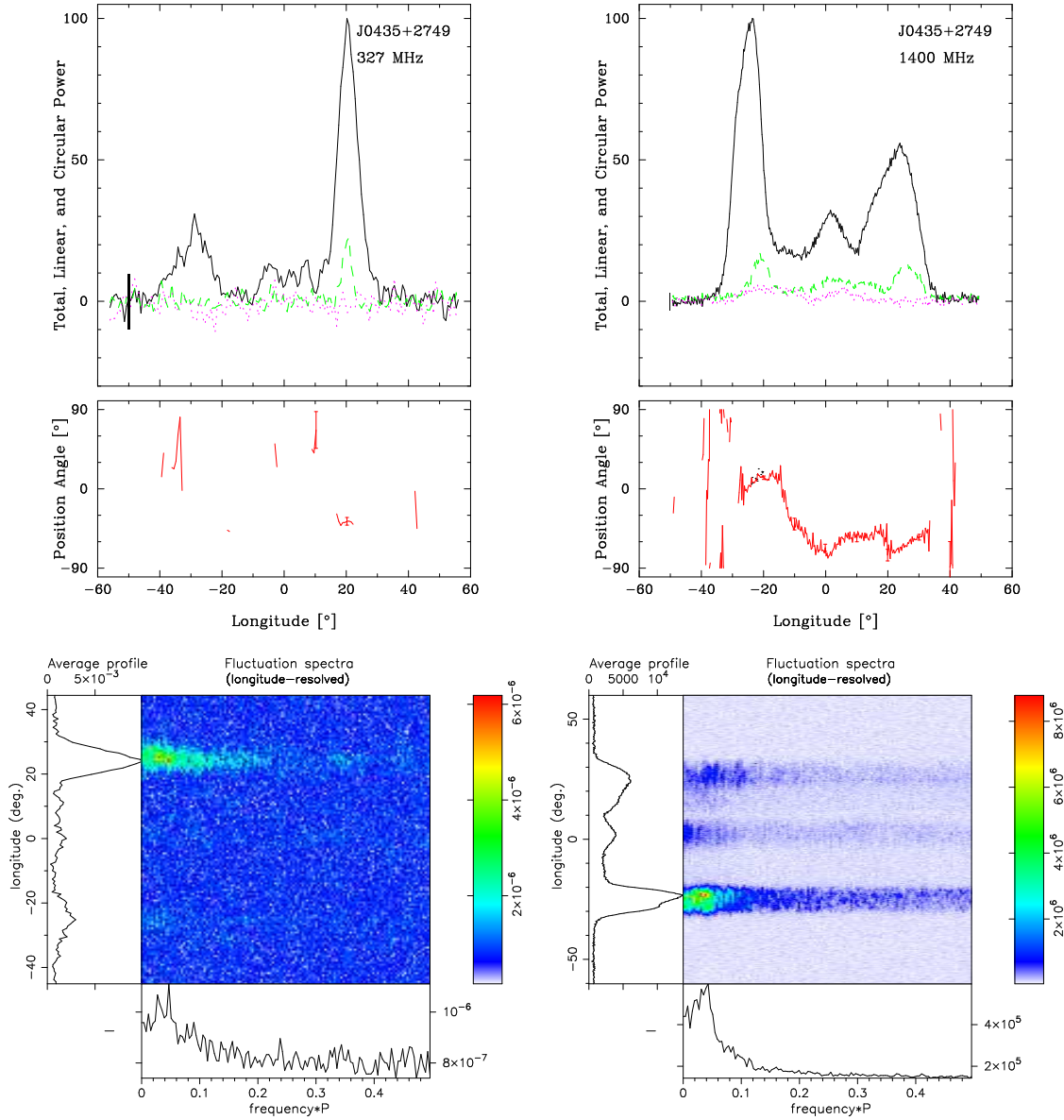


Figure A1: PSR J0435+2749 polarized profiles (upper displays) and fluctuation spectra (lower displays) at 327 MHz (left) and 1400 MHz (right). The upper panels of the polarization displays give the total intensity (Stokes  $I$ ; solid curve), the total linear ( $L (= \sqrt{Q^2 + U^2})$ ; dashed green), and the circular polarization (Stokes  $V$ ; dotted red). The PPA  $[=(1/2) \tan^{-1}(U/Q)]$  single values (dots, lower panels) in plots of the stronger pulsars correspond to those samples having errors smaller than  $2 \sigma$  in  $L$ , and the average PPA is over plotted (solid red curve) with occasional  $3\text{-}\sigma$  errors. The longitude-resolved fluctuation spectra show the power levels in the main panel according to the color bars (right). The average profiles are given in the left-hand panels and the aggregate fluctuating power in panels at the bottom of each display.

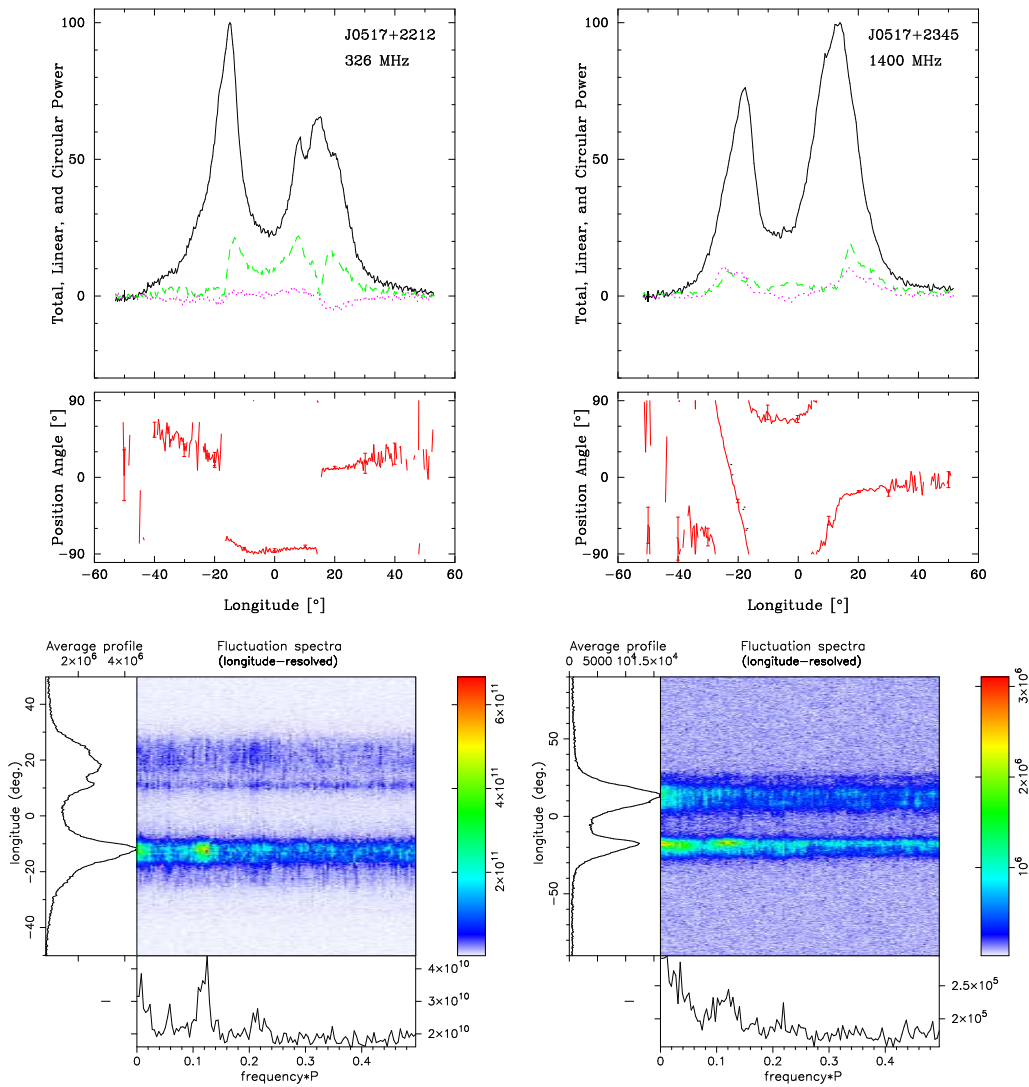


Figure A2: J0517+2345 polarized profiles and fluctuation spectra as in Fig.A1.

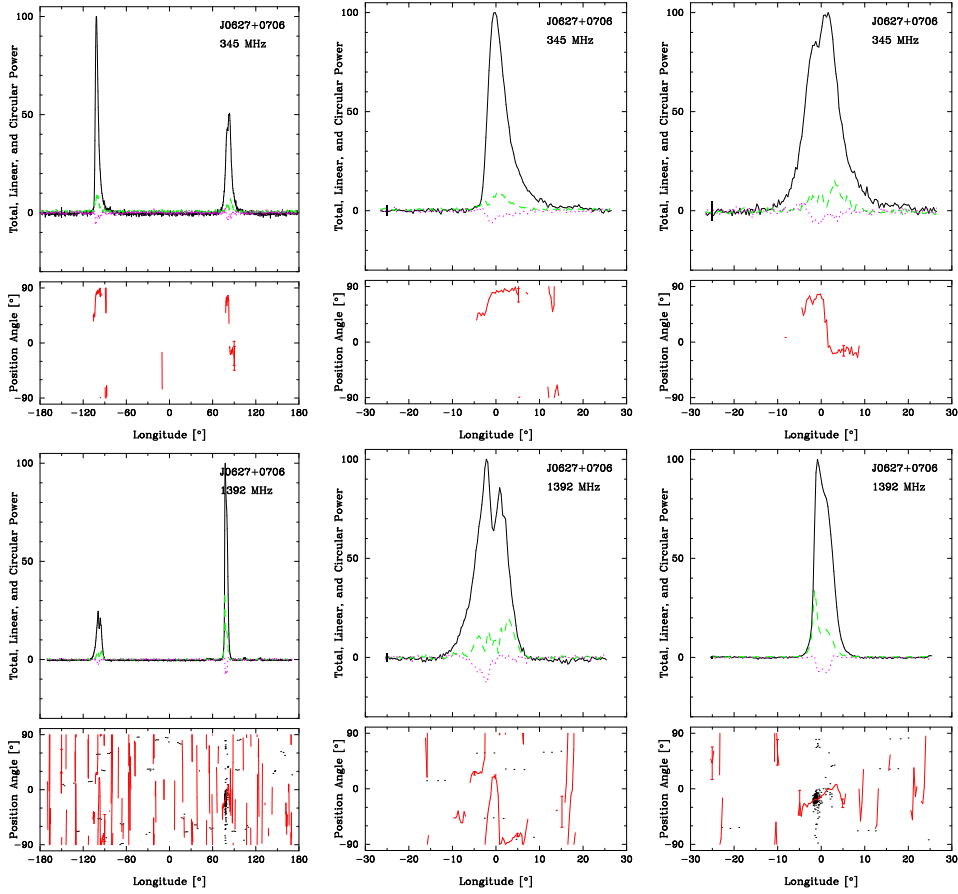


Figure A3: J0627+0706 327- (upper row) and 1400-MHz (lower row) MHz polarized profiles as in Fig.A1

. Full period displays on the left show the pulsar's main pulse and interpulse and the center and righthand plots show them separately.

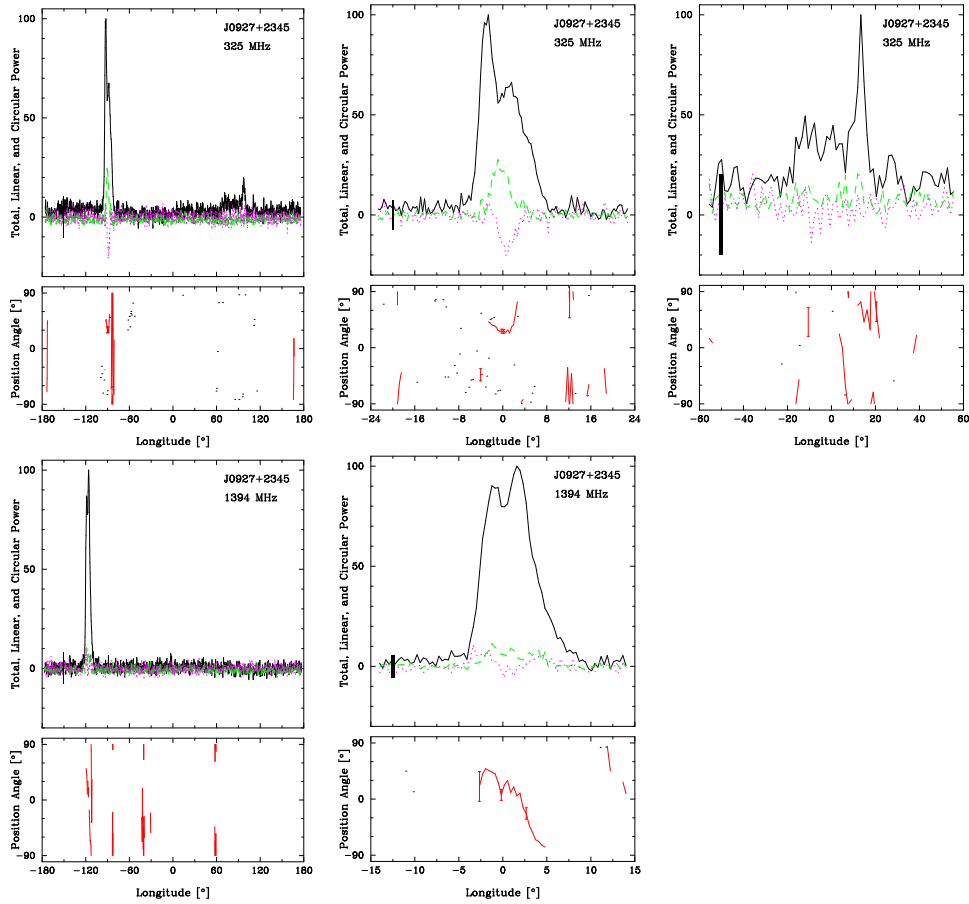


Figure A4: J0927+2345 as in Fig. 6. The pulsar's weak interpulse was not detected at the higher frequency separately.

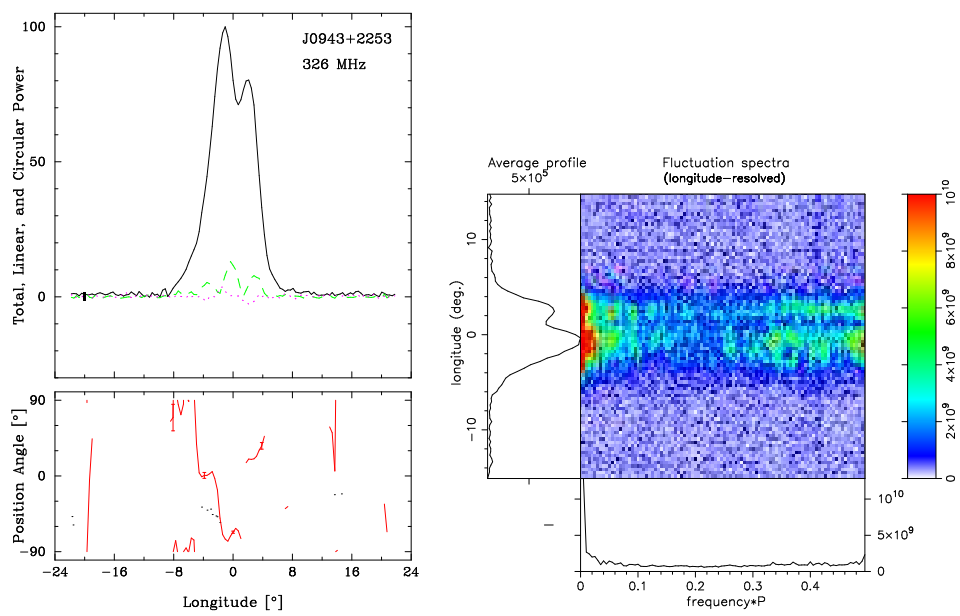


Figure A5: J0943+2253 polarized profiles and fluctuation spectra as in Fig.A1.

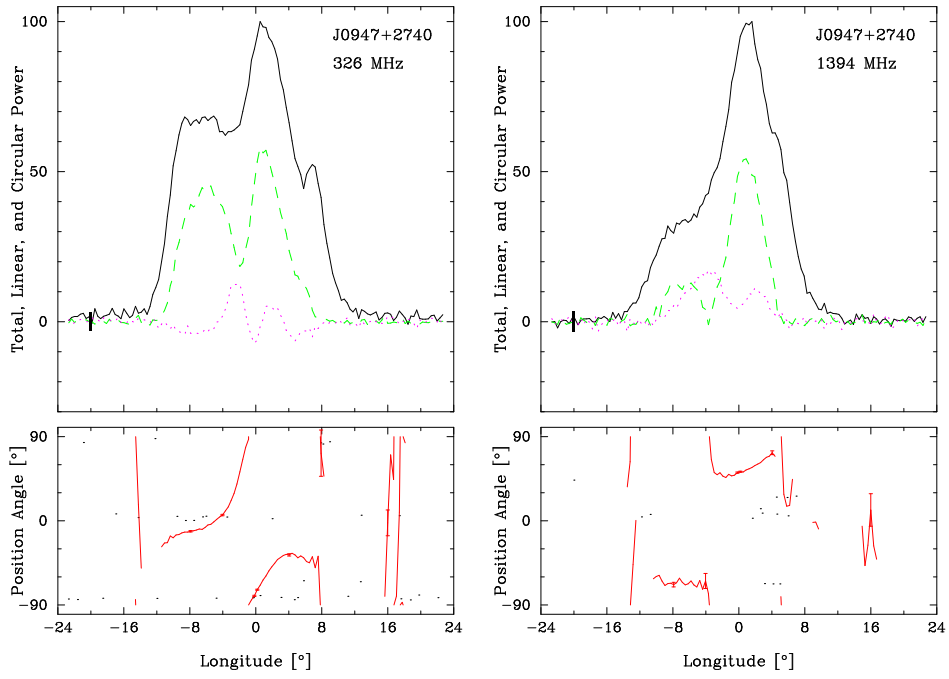


Figure A6: J0947+2740 polarized profiles as in Fig.A1.

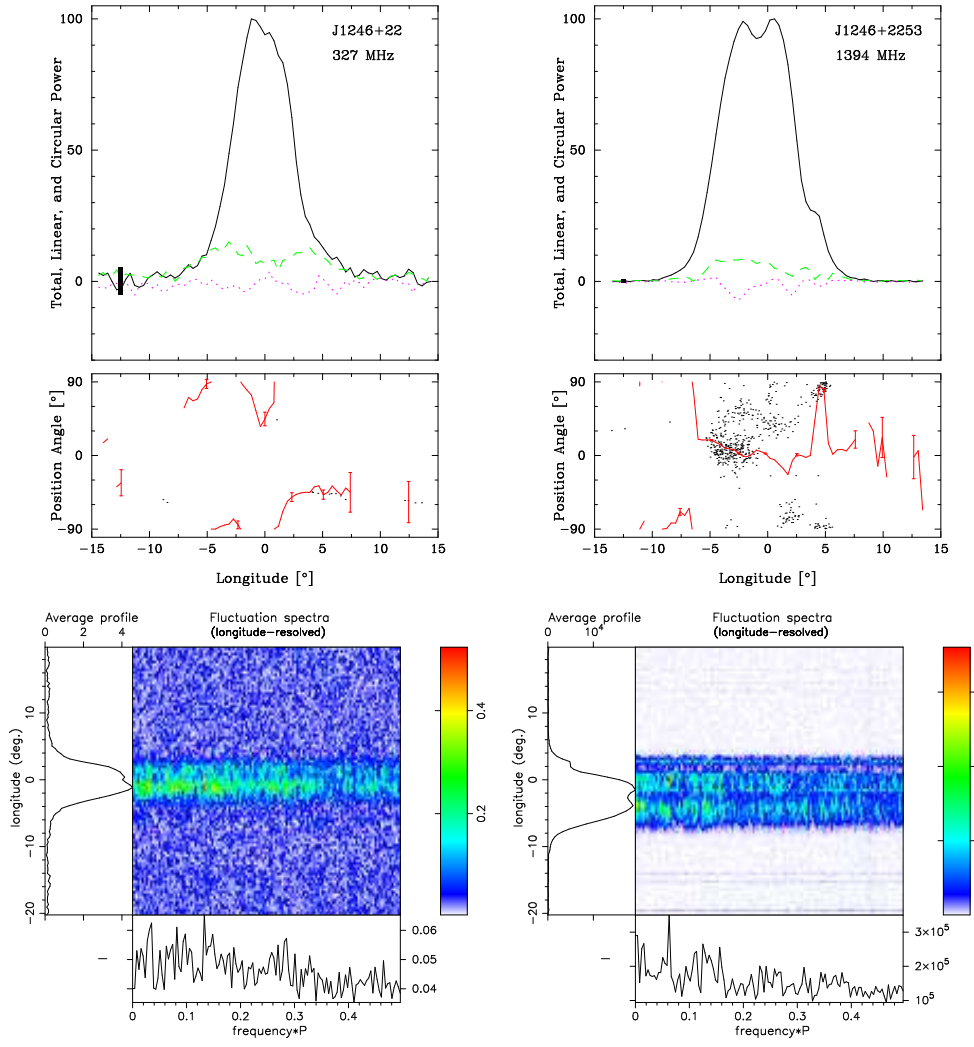


Figure A7: J1246+2253 polarized profiles and fluctuation spectra as in Fig.A1.

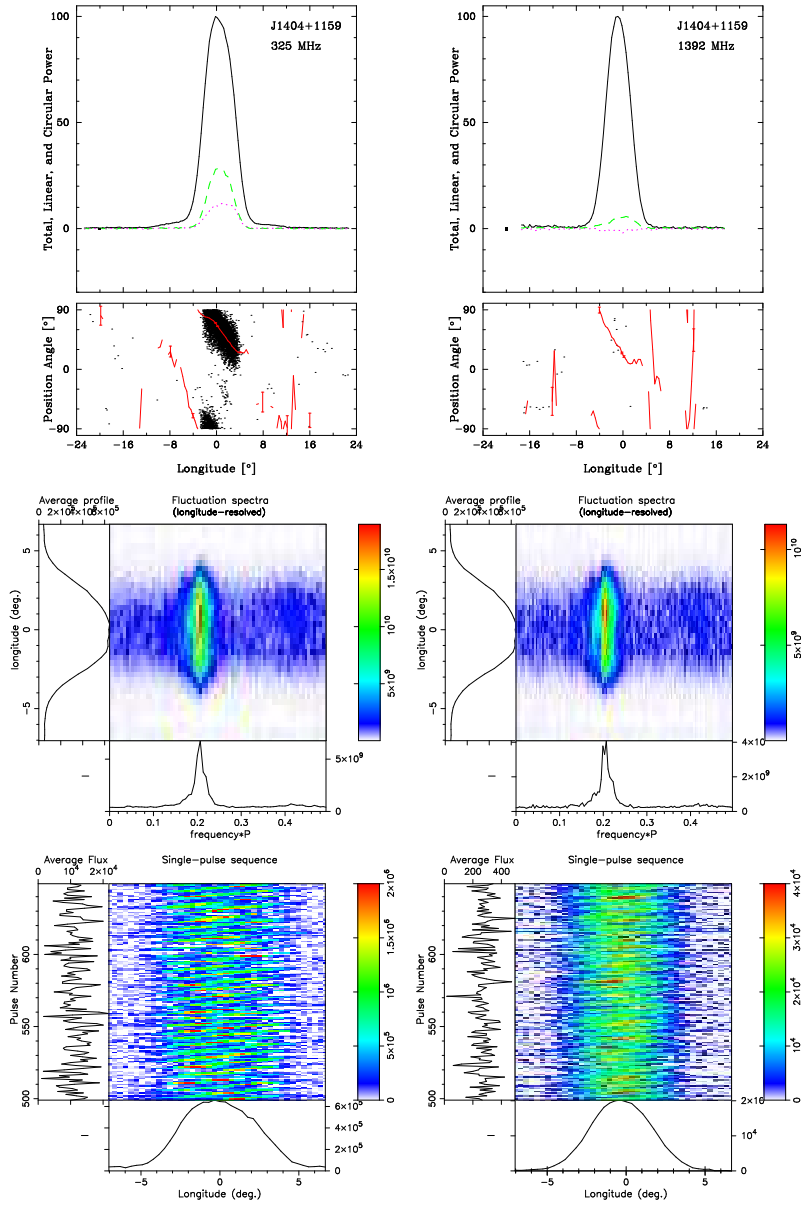


Figure A8: J1404+1159 polarized profiles and fluctuation spectrum as in Fig.A1 . Additionally, a display showing the pulsar’s accurately drifting subpulses is given along the bottom.

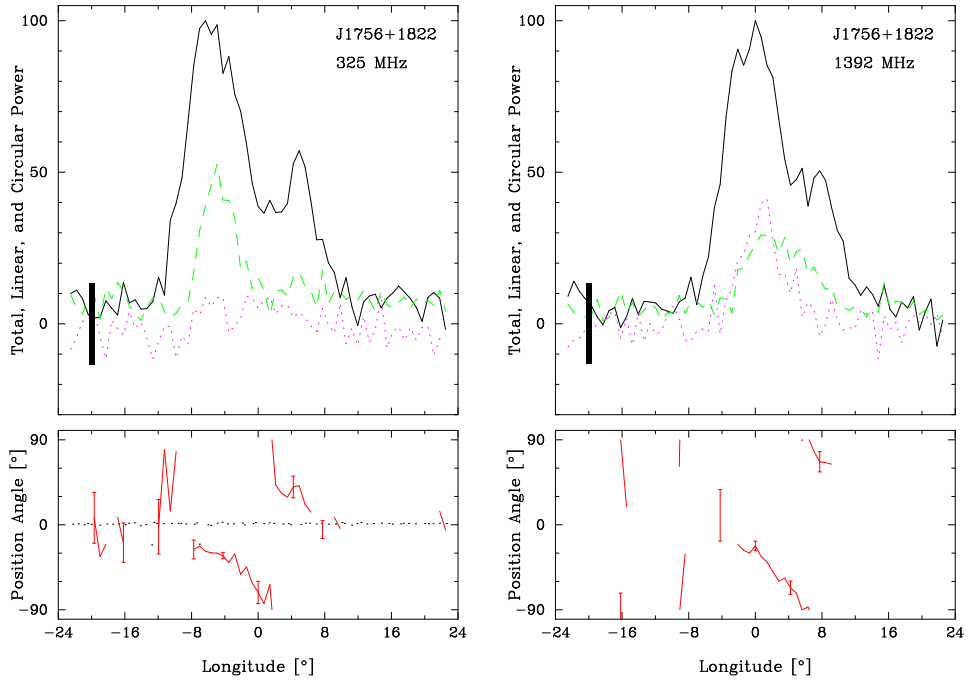


Figure A9: J1756+1822 polarized profiles as in Fig.A1.

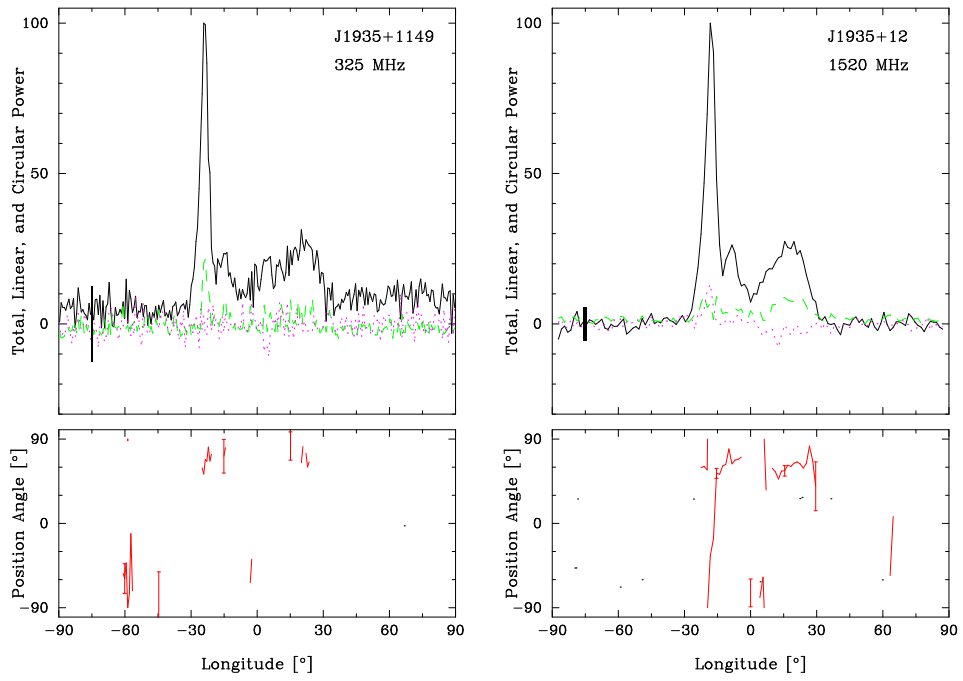


Figure A10: J1935+1159 polarized profiles as in Fig.A1.

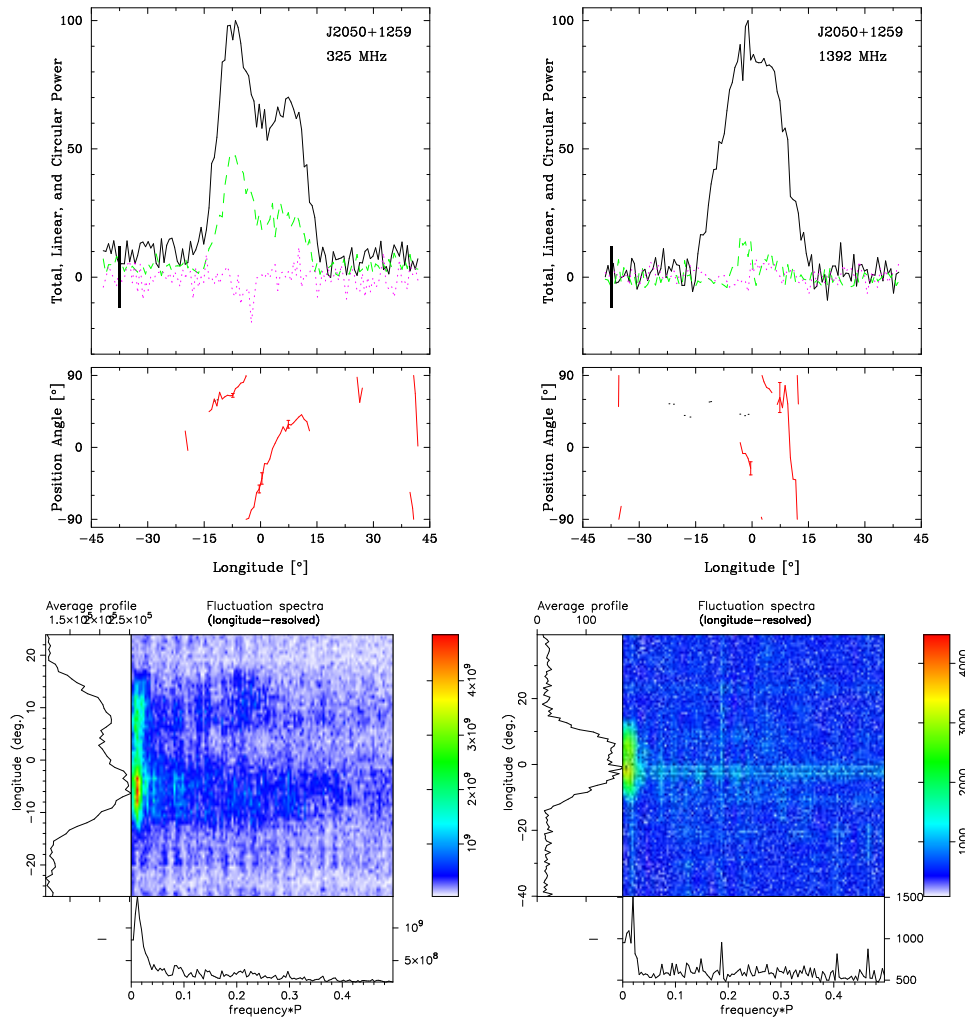


Figure A11: J2050+1259 polarized profiles and fluctuation spectra as in Fig.A1.

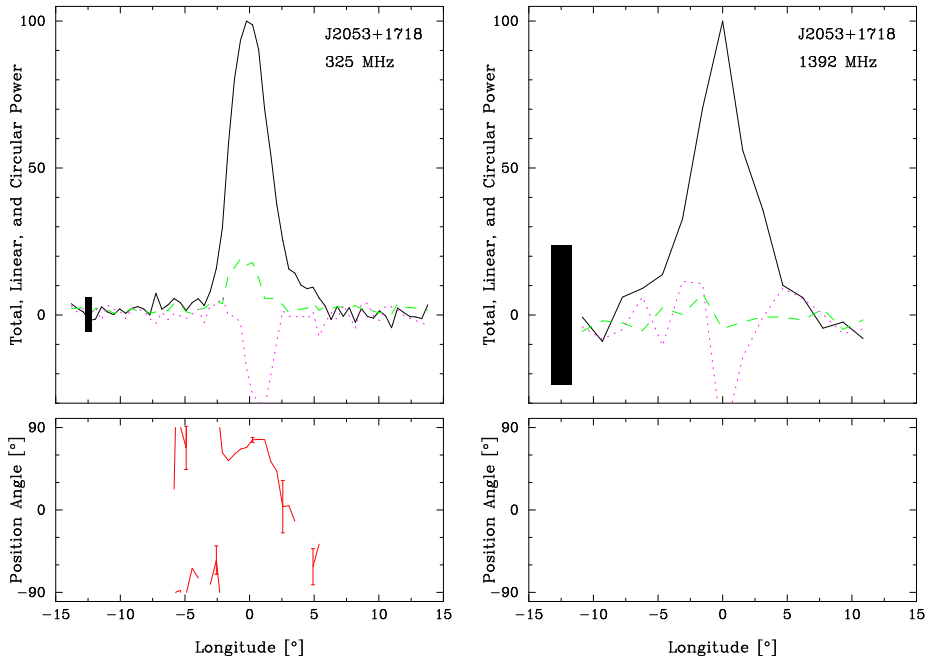


Figure A12: J2053+1718 polarized profiles as in Fig.A1.